

# Optimizing Super-resolution Reconstruction using a Genetic Algorithm

Michał Kawulok<sup>1,2</sup>, Daniel Kostrzewa<sup>1,2</sup>, Paweł Benecki<sup>1,2</sup> and Łukasz Skonieczny<sup>1</sup>

<sup>1</sup>Future Processing, Bojkowska 37A, 44-100 Gliwice, Poland

<sup>2</sup>Institute of Informatics, Silesian University of Technology, Akademicka 16, 44-100 Gliwice, Poland

**Keywords:** Genetic Algorithm, Image Processing, Super-resolution Reconstruction.

**Abstract:** Super-resolution reconstruction (SRR) is aimed at increasing spatial resolution given a single image or multiple images presenting the same scene. The existing methods are underpinned with a premise that the observed low resolution images are obtained from a hypothetical high resolution image by applying a certain imaging model (IM) which degrades the image and decreases its resolution. Hence, the reconstruction consists in applying an inverse IM to recover the high resolution data. Such an approach has been found effective, if the IM is known and controlled, in particular when the low resolution images are indeed obtained from a high resolution one. However, in a real-world scenario, when SRR is performed from images originally captured at low resolution, finding appropriate IM and tuning its hyperparameters is a challenging task. In this paper, we propose to optimize the SRR hyperparameters using a genetic algorithm, which has not been reported in the literature so far. We argue that this may substantially improve the capacities of learning the relation between low and high resolution images. Our initial, yet highly encouraging, experimental results reported in the paper allow us to outline our research pathways to deploy the developed techniques in practice.

## 1 INTRODUCTION

Effectiveness of a number of computer vision systems which include some object detection or pattern recognition tasks, strongly depends on spatial resolution of the input images. In many cases, obtaining images of sufficiently high resolution is difficult and it is subject to a number of trade-offs. They range from the cost of image acquisition to accessibility and safety (e.g., for medical imaging). Overall, this motivated the researchers to develop the algorithms that would allow a high resolution image be reconstructed from a series of images of lower spatial resolution—this process is known as *super-resolution reconstruction* (SRR) and it has gained considerable attention over the years. Despite many advancements, in many cases the state-of-the-art solutions are still insufficient to deploy SRR in practical applications.

### 1.1 Related Work

SRR was considered for a variety of computer vision problems, including medical imaging (Yang et al., 2015; Jiang et al., 2014), analysis of facial images (Jiang et al., 2014), satellite imaging (Zhu et al., 2016), document image processing (Capel and Zis-

serman, 2000), or microscopy imaging (Lukinavičius et al., 2013). SRR can be executed (i) given a single image (Demirel and Anbarjafari, 2011), (ii) from a sequence of images acquired with some shifts in the spatial domain (Li et al., 2008b), or (iii) by processing hyper-spectral images (Qian and Chen, 2012).

For single-image SRR, example-based learning (Timofte et al., 2014) is usually employed, which exploits a large collection of examples—the reconstruction consists in matching image patches between images of low and high resolution. This allows for achieving visually plausible results, but may easily lead to introducing some artifacts. The recent advancements in single-image SRR are attributed mainly to deep learning, which is being actively exploited for this purpose. Dong et al. (2016) has shown that a super-resolution convolutional neural network of relatively simple architecture outperforms the state-of-the-art example-based methods. Also, much deeper architectures coupled with fast residual training were found effective (Kim et al., 2016).

Deep networks have not been exploited for multiple-image SRR, which is considered in the research reported here. The existing methods usually employ a parametrized imaging model (IM) that simulates the process of degrading a hypothetical high-

resolution image into a set of  $N$  observed low resolution ones— $\mathbf{I}_L = \{\mathcal{I}_i^{(l)} : i \in [1..N]\}$ . In general, such models include image warping, blurring, downsampling and finally contamination with the noise (Nasrollahi and Moeslund, 2014). Some of the IM parameters are specific to each  $\mathcal{I}^{(l)}$ —basically, they stand for the differences within  $\mathbf{I}_L$  and they are concerned with the noise distribution and subpixel shifts between  $\mathcal{I}_i^{(l)}$ . SRR consists in determining these parameters given  $\mathbf{I}_L$ , which is an ill-posed optimization problem—it is usually solved by employing the Bayesian framework (Villena et al., 2004) or other optimization techniques with some regularization imposed to provide appropriate balance between sharp edges and spatial smoothness of the reconstructed high-resolution image  $\mathcal{I}^{(h)}$  (Yue et al., 2016). A thorough study on the regularization in SRR has been reported by Panagiotopoulou and Anastassopoulos (2012). Another fairly popular optimization technique applied here is the projection onto convex sets (Akgun et al., 2005), which consists in updating the high-resolution target image iteratively based on the error measured between  $\mathcal{I}^{(l)}$  and  $\mathcal{I}^{(h)}$ —a downsampled version of the reconstructed  $\mathcal{I}^{(h)}$ , degraded using the assumed IM. Among other methods, adaptive Wiener filter (Hardie, 2007) and random Markov fields (Li et al., 2008a) were used to specify the imaging model. Importantly, an IM is controlled with a set of *hyperparameters* that are common for all low-resolution images.

A commonly adopted way to evaluate the outcome of SRR is to degrade a high-resolution image  $\mathcal{I}^{(h)}$  using an IM defined on a theoretical basis to obtain the set  $\mathbf{I}_L$  (Farsiu et al., 2004). Subsequently, SRR is employed to reconstruct  $\mathcal{I}^{(h)}$  from  $\mathbf{I}_L$ , and its quality is assessed based on the similarity between  $\mathcal{I}^{(h)}$  and  $\mathcal{I}^{(h)}$ , measured with peak signal-to-noise ratio (PSNR) or structure similarity index (SSIM) (Wang et al., 2004). Such a scenario makes it possible to evaluate the optimization process, but it does not verify whether the assumed IM is appropriate. The latter is often done only qualitatively—SRR is performed for camera-captured images and the outcome is assessed visually (rather than quantitatively). Overall, the problem of selecting IM and tuning its hyperparameters has not been deeply studied in the literature and it remains an open issue.

## 1.2 Contribution

Our contribution consists in proposing a genetic algorithm (GA) to optimize the hyperparameters of an SRR process (including the IM), so as to increase its accuracy in recovering high resolution image data. Learning the relation between the images that have

been captured at different native resolution is in contrast to many works, in which the IM is assumed *a priori* and it is used to generate the validation data. In the work reported here, we initially verify the proposed concept—we validate our new algorithm (GA-SRR) by using it to optimize the hyperparameters of a well-established SRR method (Farsiu et al., 2004) applied to reconstruct artificially degraded images. Importantly, our proposed framework is fairly generic and extendable, and we outline our intended research pathways to deploy it in a realistic scenario.

## 1.3 Paper Structure

In Section 2, we present the SRR algorithm, which we exploit to validate our concept, and we explain the hyperparameters that we optimize. Our GA-SRR is demonstrated and discussed in Section 3 and our initial experimental results are reported in Section 4. Finally, in Section 5, we conclude the paper and we outline the goals of our ongoing research.

## 2 SRR FROM MULTIPLE IMAGES

The majority of multiple-image SRR methods assume that any observed image  $\mathcal{I}^{(l)}$  could be obtained from an image of higher resolution  $\mathcal{I}^{(h)}$  by applying the following generic degradation model (Yue et al., 2016):

$$\mathcal{I}_i^{(l)} = \mathbf{D}_i \mathbf{B}_i \mathbf{W}_i \mathcal{I}^{(h)} + n_i, \quad (1)$$

where  $\mathbf{W}$  is the warp matrix (it includes translation and rotation),  $\mathbf{B}$  is the blur matrix,  $\mathbf{D}$  downscales the image, and  $n$  stands for the additive noise. Importantly, if the observed images are captured by the same sensor, it may be assumed that  $\mathbf{B}$  and  $\mathbf{D}$  are common for all the images in the series (thus, they do not depend on  $i$ ). Hence, the differences among the observed images are resulting from translations and rotations, as well as from the additive noise.

A super-resolved image is found based on *maximum a posteriori* (MAP) theory as a solution ( $\mathcal{X}$ ) of a minimization problem:

$$\mathcal{I}^{(h)} = \arg \min_{\mathcal{X}} \sum_{i=1}^N \rho(\mathcal{I}_i^{(l)}, \mathbf{D} \mathbf{B} \mathbf{W}_i \mathcal{X}) + \lambda U(\mathcal{X}), \quad (2)$$

where  $\rho(\cdot)$  is an image similarity metric and  $U(\cdot)$  is the regularization term. The existing SRR methods present different approaches towards defining the degradation matrices, regularization terms and optimization techniques.

For our proof of concept, we selected the method proposed by Farsiu et al. (2004). They exploit the  $L_1$  norm to measure the similarity  $\rho$ ,  $\mathbf{B}$  matrix implements the Gaussian blur, and for regularization, the total variation method (Rudin et al., 1992) is combined with a bilateral filter:

$$U(\mathcal{X}) = \sum_{l=-P}^P \sum_{m=-P}^P \alpha^{|m|+|l|} \left\| \mathcal{X} - \mathbf{S}_y^m \mathbf{S}_x^l \mathcal{X} \right\|_1, \quad (3)$$

where  $\mathbf{S}_x^l$  and  $\mathbf{S}_y^m$  shift an image by  $l$  and  $m$  pixels in horizontal and vertical direction, respectively, and  $0 < \alpha < 1$  is a parameter of spatial decay. The reconstructed image is obtained by minimizing the term (2), which is done with the iterative steepest gradient descent—the update is obtained as

$$\mathcal{X}_{n+1} = \mathcal{X}_n - \beta \left( \frac{d\rho}{d\mathcal{X}}(\mathcal{X}_n) + \lambda \frac{dU}{d\mathcal{X}}(\mathcal{X}_n) \right), \quad (4)$$

where

$$\frac{d\rho}{d\mathcal{X}}(\mathcal{X}_n) = \sum_{i=1}^N \mathbf{W}_i^T \mathbf{B}^T \mathbf{D} \text{sgn}(\mathbf{D} \mathbf{B} \mathbf{W}_i \mathcal{X}_n - \mathcal{I}_i^{(l)}), \quad (5)$$

$$\frac{dU}{d\mathcal{X}}(\mathcal{X}_n) = \sum_l \sum_m \alpha^{|m|+|l|} \mathbf{S}' \text{sgn}(\mathcal{X}_n - \mathbf{S}_y^m \mathbf{S}_x^l \mathcal{X}_n), \quad (6)$$

$$\mathbf{S}' = \mathbf{1} - \mathbf{S}_y^{-m} \mathbf{S}_x^{-l}. \quad (7)$$

Overall, the SRR process is controlled with (i) a single parameter ( $\sigma$ ) that defines the width of the Gaussian kernel used in  $\mathbf{B}$ , (ii)  $P$  used in the regularization (3), and (iii) the remaining hyperparameters related to the optimization process (4)–(7), namely:  $\alpha$ ,  $\beta$ ,  $\lambda$  and the number of gradient descent iterations ( $\Gamma$ ). It is worth noting that Farsiu et al. (2004) applied their SRR method to several images, for each of which different values of the hyperparameters were found optimal. The parameters specific to every single presented image  $\mathcal{I}_i^{(l)} \in \mathbf{I}_L$  are concerned with the  $\mathbf{W}_i$  matrix, and they are determined by subpixel registration of the images within each  $\mathbf{I}_L$ . This is done prior to the SRR process and the values in  $\mathbf{W}_i$  remain fixed afterwards.

### 3 GENETIC ALGORITHM TO OPTIMIZE SRR

SRR algorithms are controlled with a number of hyperparameters, which severely influence the quality of the reconstructed image, and the problem of their tuning has been paid little attention in the literature so far. Therefore, we expect a framework for optimizing these hyperparameters to improve the capacities of

existing SRR methods, and hopefully this may lead to developing adaptive IMs that could better reflect the relation between images of low and high spatial resolution. Motivated by that, we explore the possibilities of applying a GA to optimize the SRR hyperparameters. In the research reported here, we demonstrate that the proposed GA-SRR algorithm is successful in optimizing a well-established SRR technique (Farsiu et al., 2004). Importantly, the essential components of our framework are thought to be highly generic, hence we intend to embrace other SRR methods, which is discussed later in Section 5.

#### 3.1 Outline of GA-SRR

The pseudocode of the proposed algorithm is presented in Alg. 1. A population  $\mathcal{P}$  of  $N_P$  individuals is initialized (line 1)—a chromosome of each individual defines the values of hyperparameters which control the SRR process (these values are initialized randomly within an allowed range specific to each hyperparameter). Subsequently, each individual in  $\mathcal{P}$  is considered for mutation with the probability  $P_m$  and the selected individuals ( $\mathcal{P}_M$ ) are excluded from the individuals selected for crossover ( $\mathcal{P}_C$ ) (lines 3–4). The individuals in  $\mathcal{P}_C$  are paired and crossed over to create an offspring population  $\mathcal{P}'_C$  of the same size as  $\mathcal{P}_C$ , hence  $\#\mathcal{P}_C = \#\mathcal{P}'_C$ . During crossover (line 5) of two individuals  $p_a$  and  $p_b$ , each parameter value of the child  $p_{a+b}$  is copied either from  $p_a$  or  $p_b$  with equal probability. For each individual selected for mutation, one value in the chromosome is selected and modified within the allowed range (line 6). The existing population  $\mathcal{P}$  is appended with the mutated individuals  $\mathcal{P}'_M$  and those created during the crossover ( $\mathcal{P}'_C$ )—this creates a new population  $\mathcal{P}'$  (line 7). Fitness  $\eta$  of each new solution is retrieved (this is explained later in Section 3.2) to select the  $N_P$  fittest individuals (line 11). When the stop condition is met (line 13), the best solution  $p_B$  is returned (line 14), which configures the SRR method.

#### 3.2 Computing the Fitness

The process to retrieve the fitness  $\eta$  of an individual  $p_i$  is illustrated in Fig. 1a. Basically, this process requires a set of  $M$  high-resolution images, each of which is coupled with a set of low-resolution counterparts  $\mathbf{I}_L$ —an example is presented in Fig. 1b (here, four low-resolution images in  $\mathbf{I}_L$  present the same region as a high-resolution image  $\mathcal{I}^{(h)}$ ).

To evaluate the fitness  $\eta$  of an individual  $p_i$ , the hyperparameters defined by its chromosome are used to configure the SRR process, which is run to pro-

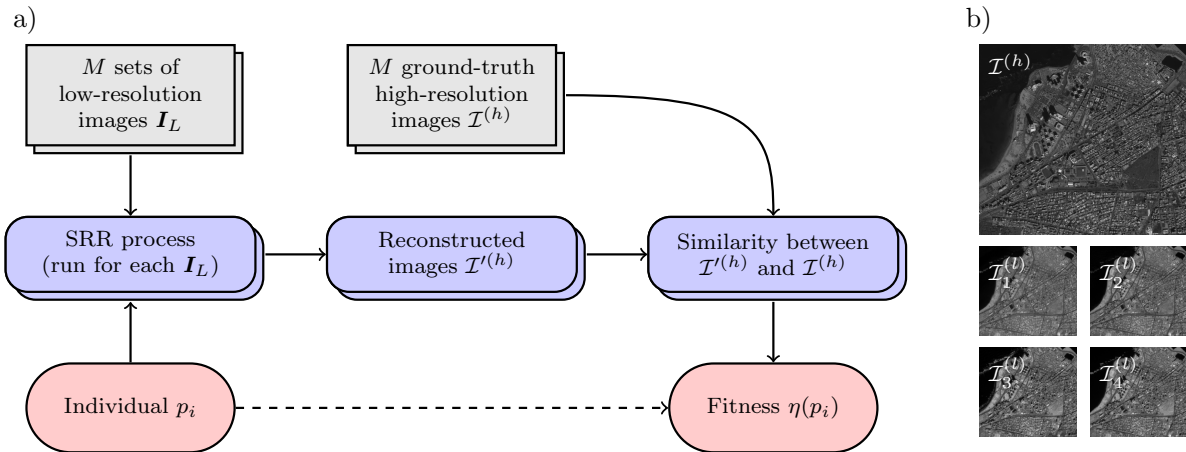


Figure 1: The process of computing the fitness  $\eta(p_i)$  of an individual  $p_i$  (a) along with an example of input images of low ( $I_i^{(l)}$ ) and high ( $I^{(h)}$ ) resolution (b).

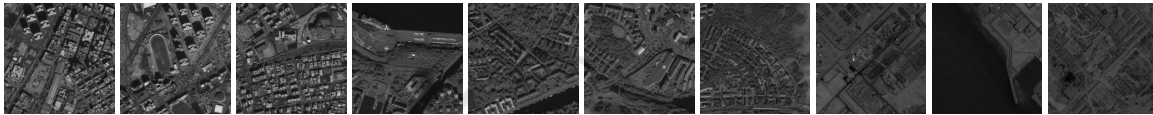


Figure 2: Images used to train GA-SRR.

**Algorithm 1** A genetic algorithm for optimizing SRR hyperparameters (GA-SRR).

- 1: Initialize population  $\mathcal{P} = \{p_i\}$  of size  $N_P$ ;
- 2: **repeat**
- 3:  $\mathcal{P}_M \leftarrow \text{SELECTFORMUTATION}(\mathcal{P}, P_m)$ ;
- 4:  $\mathcal{P}_C \leftarrow \mathcal{P} \setminus \mathcal{P}_M$ ;
- 5:  $\mathcal{P}'_C \leftarrow \text{CROSSOVER}(\mathcal{P}_C)$ ;
- 6:  $\mathcal{P}'_M \leftarrow \text{MUTATE}(\mathcal{P}_M)$ ;
- 7:  $\mathcal{P}' \leftarrow \mathcal{P} \cup \mathcal{P}'_M \cup \mathcal{P}'_C$ ;
- 8: **for all**  $\{p_i\} \in \mathcal{P}'$  **do**
- 9:  $\eta(p_i) \leftarrow \text{FITNESS}(p_i)$ ;
- 10: **end for**
- 11:  $\mathcal{P} \leftarrow \text{SELECT}(\mathcal{P}', N_P)$ ;
- 12:  $p_B \leftarrow \arg \max_{p_i \in \mathcal{P}} \{\eta(p_i)\}$ ;
- 13: **until** STOPCONDITION;
- 14: **return** ( $p_B$ );

cess each  $I_L$  and reconstruct a high-resolution image  $I'^{(h)}$ . Quality of the reconstruction is assessed based on the similarity between  $I'^{(h)}$  and  $I^{(h)}$ , measured with SSIM. The final fitness  $\eta(p_i)$  is obtained as the mean of  $M$  similarity scores—basically, the better the SRR is, the more similar is the reconstructed image to the ground truth, and this similarity is expected to increase during the evolutionary optimization.

## 4 EXPERIMENTAL VALIDATION

In order to verify the capacities of the proposed approach to optimize the SRR hyperparameters, we have run an experiment in a controlled environment for  $M = 10$  artificially degraded satellite images of  $200 \times 200$  pixels, presented in Fig. 2. Each high-resolution image  $I^{(h)}$  was subject to a small translation, followed by the Gaussian blur, and downsampled to  $100 \times 100$  pixels—for each  $I^{(h)}$ , we generated  $N = 25$  downsampled images  $I^{(l)}$ . From these images, we reconstruct the high-resolution image using the algorithm by Farsiu et al. (2004), whose hyperparameters are optimized with GA-SRR. The values of the hyperparameters were initialized in the following ranges, set based on the results reported in the paper (Farsiu et al., 2004):  $\alpha \in (0, 1)$ ,  $\beta \in (0, 200)$ ,  $\lambda \in (0, 0.2)$ ,  $\Gamma \in [1, 20]$ ,  $\sigma \in (0, 5)$  and  $P \in [1, 5]$ . We implemented the algorithms in C++ (using OpenCV library) and we ran the experiments on an Intel Xeon 3.2 GHz computer with 16 GB RAM.

As our goal here was to verify the behavior of the genetic algorithm, we observed the fitness (i.e., the average SSIM for  $M$  samples) in subsequent iterations of the GA optimization. We ran the process 10 times and we stop the optimization after 10 iterations (which we found sufficient to verify the concept). Average and best fitness in subsequent itera-

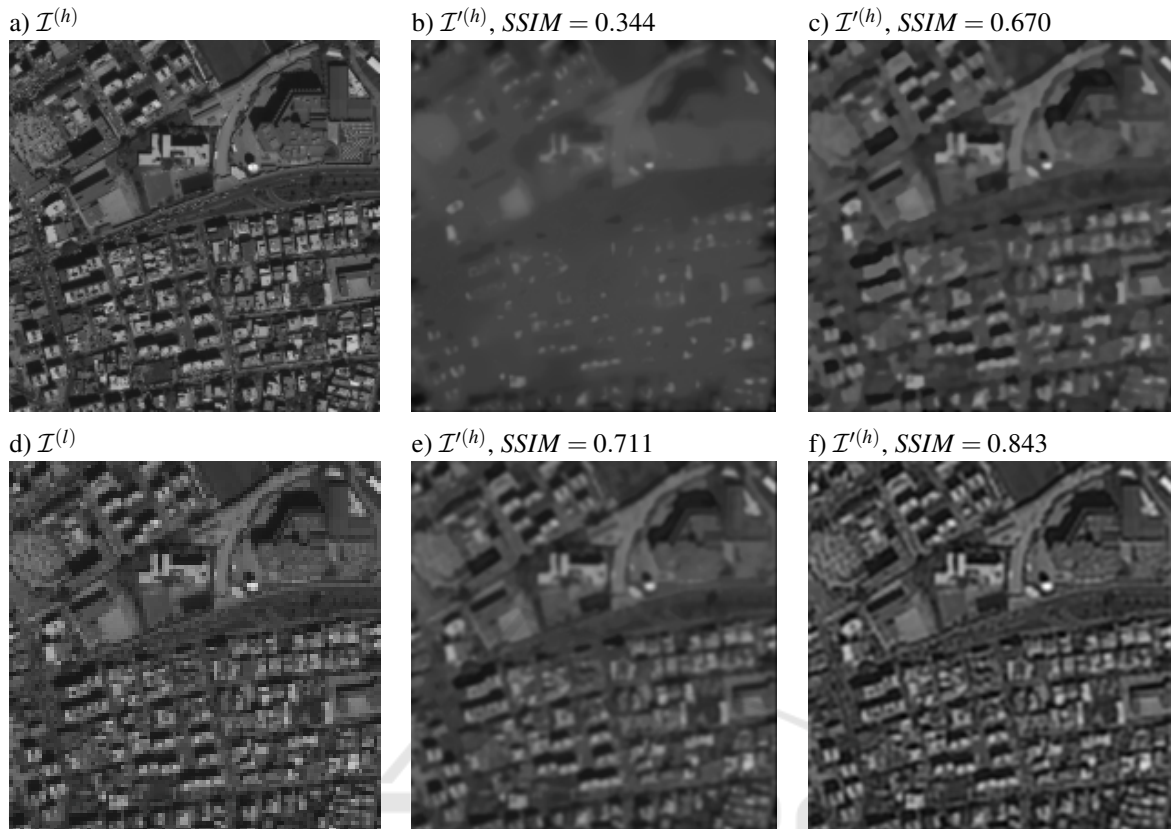


Figure 4: Examples of an image from the training set: a)  $\mathcal{I}^{(h)}$ ,  $\mathcal{I}^{(l)}$  and reconstructed  $\mathcal{I}'^{(h)}$  using different hyperparameters.

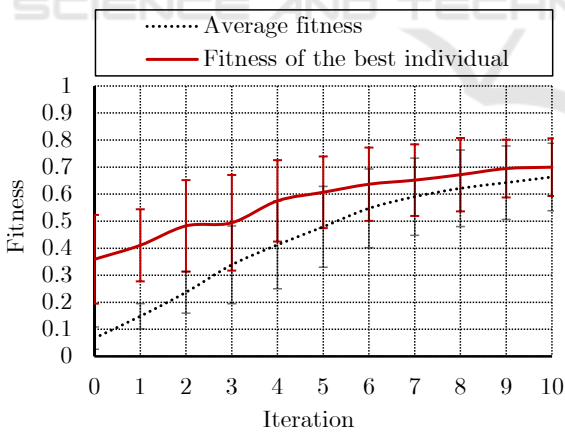


Figure 3: Average and best fitness in subsequent generations of GA-SRR.

tions along with the standard deviation are presented in Fig. 3. It may be seen that the SRR quality grows during the optimization and the standard deviation of the best fitness decreases, which confirms the convergence capabilities of the proposed GA. In addition, we inspected the results qualitatively—an example of the reconstruction improvement during the GA opti-

mization is presented in Fig. 4. The figure presents the input  $\mathcal{I}^{(h)}$  and  $\mathcal{I}^{(l)}$  images (a, d) alongside four examples of  $\mathcal{I}'^{(h)}$  obtained within a single run of GA-SRR (b, c, e, f). It may be seen that during the optimization process, the reconstruction quality improves both quantitatively and qualitatively. For low *SSIM* values (b, c), it may be concluded that the regularization is too strong, which results in observing less details than in the input low-resolution image  $\mathcal{I}^{(l)}$ . Importantly, the final image (f) contains much more details than  $\mathcal{I}^{(l)}$ , though still less than the original  $\mathcal{I}^{(h)}$  image (a)—however, this is obtained after only 10 generations of the GA. It is worth noting that the ranges of hyperparameter values are based on the results reported in the literature—overall, this indicates high sensitivity of the reconstruction process to its parameters and confirms that determining their optimal values is not a trivial task.

Although we have not run multi-fold cross-validation tests at this stage of our research, we applied the hyperparameters obtained at subsequent GA-SRR iterations (we exploited the best run out of the 10 performed) to reconstruct images that were not included in the data set used for training. This allowed

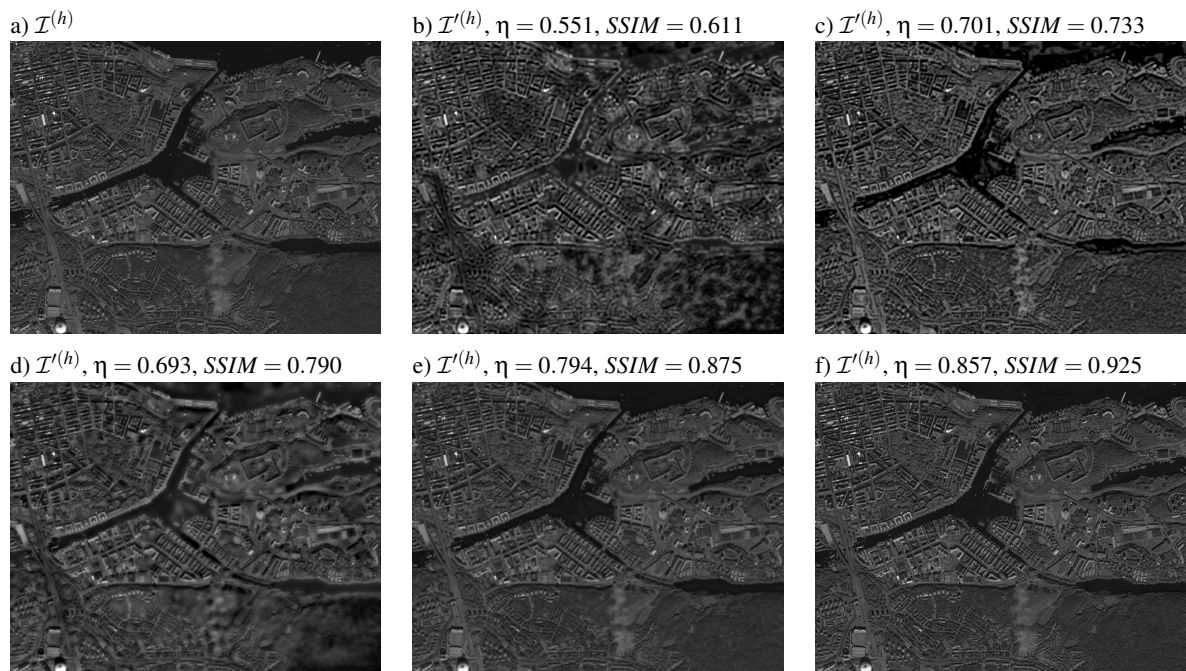


Figure 5: Example of the SRR applied to an image not included in the training set: ground-truth  $\mathcal{I}^{(h)}$  (a) and five reconstructed  $\mathcal{I}'^{(h)}$  obtained using different hyperparameters obtained during GA-SRR process (b–f).

us to initially verify the universality of the optimized hyperparameters. An example of such an image is presented in Fig. 5. It is worth noting that the values of *SSIM* measured between the original  $\mathcal{I}^{(h)}$  and reconstructed  $\mathcal{I}'^{(h)}$  present the same tendency as the fitness  $\eta$ . Importantly, the best reconstruction result (f) presents similar detail level to that visible in the original image (a), rendering *SSIM* = 0.925.

## 5 CONCLUSIONS AND FUTURE WORK

In this paper, we report our initial study on using GAs for optimizing the SRR hyperparameters. This is an important problem, as both the IM assumed for reconstruction, as well as the reconstruction process itself are sensitive to their parameters. Here, we demonstrated that the proposed GA-SRR framework is capable of optimizing a well-established SRR method. Although the tests were run for artificially degraded images rather than for images originally captured at different resolution (still, such validation scenario is commonly adopted in the state-of-the-art works on SRR), the obtained results confirm that the general idea standing behind our approach is correct. This, in turn, allows us to outline the further research steps towards addressing more realistic scenarios.

The main goal of our ongoing research is to exploit the proposed framework to configure both an IM, so that it reflects the relation between images originally captured at low and high resolution, as well as the hyperparameters of an SRR method which is based on that IM. This will allow us to adapt an IM given a training set of low and high-resolution images, captured using two different sensors (e.g., Sentinel-2 and SPOT satellites, respectively)—afterwards, the learned IM would be suitable for increasing the resolution of images having similar characteristics as those in the training set (i.e., Sentinel-2 images, referring to the given example). Obviously, the ground-truth high-resolution images will be required only for training to define the IM.

Creating such a solution will require solving several problems. First of all, we will make the IM more configurable (at this stage only the width of the Gaussian kernel is considered) to make it capable of modeling the real-life downsampling process. As a consequence, appropriate SRR method needs to be selected that will be appropriate to optimize the IM parameters for each presented sample. Another important issue is concerned with measuring the similarity between  $\mathcal{I}^{(h)}$  and  $\mathcal{I}'^{(h)}$ . In the reported study,  $\mathcal{I}'^{(h)}$  is reconstructed from the set  $\mathbf{I}_L$ , obtained from  $\mathcal{I}^{(h)}$ , which is used as the ground truth, hence the differences between  $\mathcal{I}^{(h)}$  and  $\mathcal{I}'^{(h)}$  originate only from applying the IM fol-

lowed by the reconstruction process. While simple measures (like PSNR or SSIM) are sufficient here, it is much more challenging to measure the similarity between images that have been captured using different sensors, at various spatial resolution. An example of such images was shown earlier in Fig. 1b— $\mathcal{I}^{(h)}$  and  $\mathcal{I}_i^{(l)}$  were captured by different satellites, and certainly the reconstructed image would be visually different from  $\mathcal{I}^{(h)}$ . Importantly, the differences related to the detail level may be negligible compared with those incurred by the global variations. We have found the keypoint detectors to be quite promising here (Kawulok et al., 2017) and we will consider employing them to evaluate the fitness. Overall, we currently explore how to exploit the proposed framework to adapt an IM alongside an SRR technique to images acquired by a given sensor, which will be an important step towards deploying SRR in real-life scenarios.

## ACKNOWLEDGEMENTS

The reported work is a part of the SISPARE project run by Future Processing and funded by European Space Agency. In addition, the authors were partially supported by Institute of Informatics funds no. BK-230/RAu2/2017 (MK) and BKM-509/RAu2/2017 (DK).

## REFERENCES

- Akgun, T., Altunbasak, Y., and Mersereau, R. M. (2005). Super-resolution reconstruction of hyperspectral images. *IEEE Trans Image Process*, 14(11):1860–1875.
- Capel, D. and Zisserman, A. (2000). Super-resolution enhancement of text image sequences. In *Proc. IEEE ICPR*, volume 1, pages 600–605.
- Demirel, H. and Anbarjafari, G. (2011). Discrete wavelet transform-based satellite image resolution enhancement. *IEEE Trans Geoscience and Remote Sensing*, 49(6):1997–2004.
- Dong, C., Loy, C. C., He, K., and Tang, X. (2016). Image super-resolution using deep convolutional networks. *IEEE Trans Pattern Anal and Mach Intell*, 38(2):295–307.
- Farsiu, S., Robinson, M. D., Elad, M., and Milanfar, P. (2004). Fast and robust multiframe super resolution. *IEEE Trans Image Process*, 13(10):1327–1344.
- Hardie, R. (2007). A fast image super-resolution algorithm using an adaptive wiener filter. *IEEE Trans Image Process*, 16(12):2953–2964.
- Jiang, J., Hu, R., Wang, Z., and Han, Z. (2014). Face super-resolution via multilayer locality-constrained iterative neighbor embedding and intermediate dictionary learning. *IEEE Trans Image Process*, 23(10):4220–4231.
- Kawulok, M., Kostrzewa, D., Benecki, P., and Skonieczny, L. (2017). Evaluating super-resolution reconstruction of satellite images. In *Proc. IAC 2017*, pages 1–8. IAF.
- Kim, J., Kwon Lee, J., and Mu Lee, K. (2016). Accurate image super-resolution using very deep convolutional networks. In *Proc. IEEE CVPR*, pages 1646–1654.
- Li, F., Jia, X., and Fraser, D. (2008a). Universal HMT based super resolution for remote sensing images. In *Proc. IEEE ICIP*, pages 333–336.
- Li, L., Zhang, Y., and Tian, Q. (2008b). Multi-face location on embedded dsp image processing system. In *Proc. CISP*, volume 4, pages 124–128.
- Lukinavičius, G., Umezawa, K., Olivier, N., et al. (2013). A near-infrared fluorophore for live-cell super-resolution microscopy of cellular proteins. *Nature Chemistry*, 5(2):132–139.
- Nasrollahi, K. and Moeslund, T. B. (2014). Super-resolution: a comprehensive survey. *Mach Vis and App*, 25(6):1423–1468.
- Panagiotopoulou, A. and Anastassopoulos, V. (2012). Super-resolution image reconstruction techniques: Trade-offs between the data-fidelity and regularization terms. *Inform Fusion*, 13(3):185–195.
- Qian, S.-E. and Chen, G. (2012). Enhancing spatial resolution of hyperspectral imagery using sensor’s intrinsic keystone distortion. *IEEE Trans Geoscience and Remote Sensing*, 50(12):5033–5048.
- Rudin, L. I., Osher, S., and Fatemi, E. (1992). Nonlinear total variation based noise removal algorithms. *Phys. D*, 60(1-4):259–268.
- Timofte, R., De Smet, V., and Van Gool, L. (2014). A+: Adjusted anchored neighborhood regression for fast super-resolution. In *Proc. ACCV*, pages 111–126. Springer.
- Villena, S., Abad, J., Molina, R., and Katsaggelos, A. K. (2004). Estimation of high resolution images and registration parameters from low resolution observations. *Proc. CIARP*, pages 509–516.
- Wang, Z., Bovik, A. C., Sheikh, H. R., and Simoncelli, E. P. (2004). Image quality assessment: from error visibility to structural similarity. *IEEE Trans Image Process*, pages 600–612.
- Yang, F., Chen, Y., Wang, R., and Zhang, Q. (2015). Super-resolution microwave imaging: Time-domain tomography using highly accurate evolutionary optimization method. In *Proc. IEEE EuCAP*, pages 1–4.
- Yue, L., Shen, H., Li, J., Yuan, Q., Zhang, H., and Zhang, L. (2016). Image super-resolution: The techniques, applications, and future. *Signal Process*, 128:389–408.
- Zhu, H., Song, W., Tan, H., Wang, J., and Jia, D. (2016). Super resolution reconstruction based on adaptive detail enhancement for ZY-3 satellite images. *Proc. ISPRS Annals*, pages 213–217.